iScience

CellPress

Article

Endogenous H_2S-Triggered *In Situ* Synthesis of NIR-II-Emitting Nanoprobe for *In Vivo* Intelligently Lighting Up Colorectal Cancer

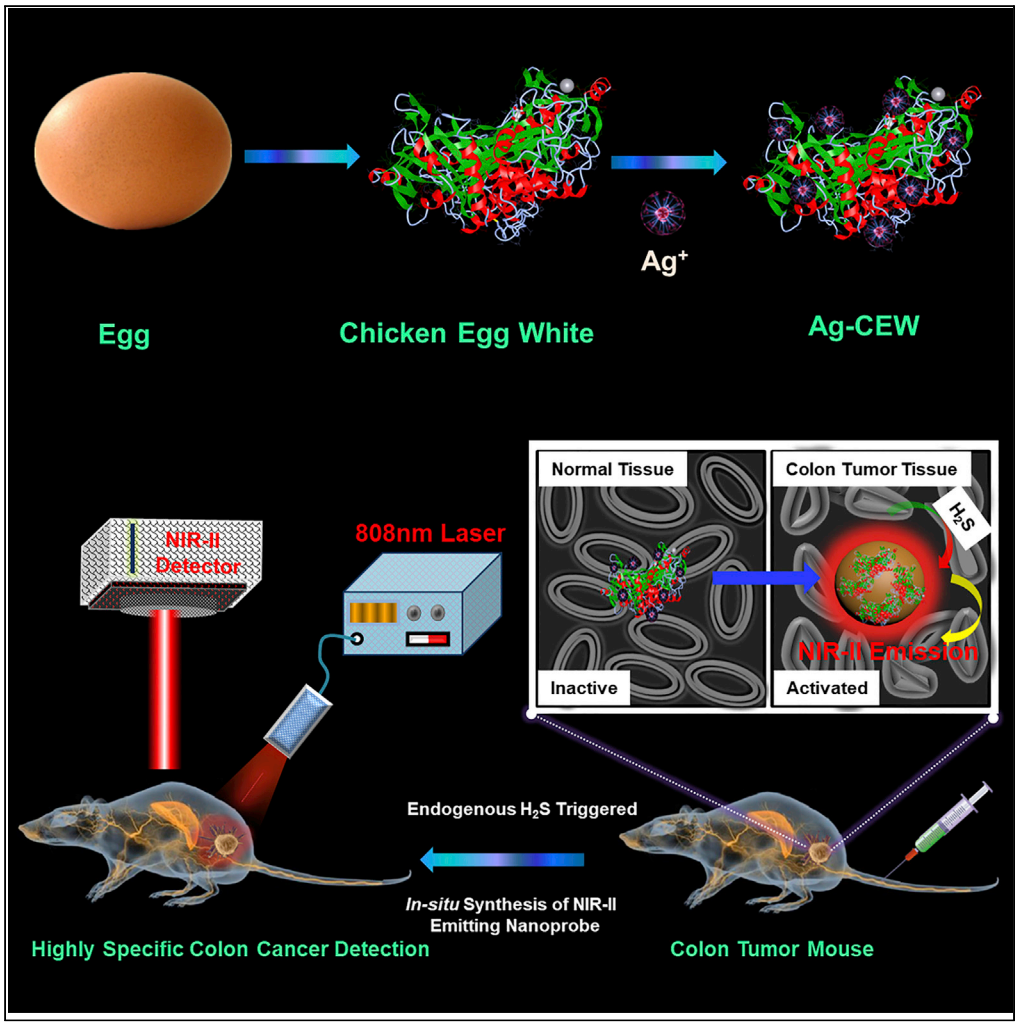

Zhiming Deng, Mingyang Jiang, Youbin Li, Hongrong Liu, Songjun Zeng, Jianhua Hao

songjunz@hunnu.edu.cn (S.Z.)
jh.hao@polyu.edu.hk (J.H.)

HIGHLIGHTS

In situ H_2S-activated Ag-CEW probe was designed for specific colon cancer diagnosis

The Ag-CEW probe triggered by H_2S presents highly efficient NIR-II emission

The activatable probe can significantly improve the sensitivity of optical imaging

Ag-CEW can completely eliminate the interference signal from liver and spleen

Deng et al., iScience 17, 217–224
July 26, 2019
https://doi.org/10.1016/j.isci.2019.06.034

iScience

CellPress

Article

Endogenous H_2S-Triggered *In Situ* Synthesis of NIR-II-Emitting Nanoprobe for *In Vivo* Intelligently Lighting Up Colorectal Cancer

Zhiming Deng,[1] Mingyang Jiang,[1] Youbin Li,[1] Hongrong Liu,[1] Songjun Zeng,[1,*] and Jianhua Hao[2,3,*]

SUMMARY

Overexpression of endogenous H_2S is one of the key characteristic in colon cancer. However, developing endogenous H_2S-activated optical probes for specific diagnosis of colorectal cancer is rarely explored. Herein, an *in situ* H_2S-activatable second near-infrared (NIR-II)-emitting nanoprobe based on Ag-chicken egg white (Ag-CEW) complex for intelligently lighting up colorectal cancer was explored. The designed Ag-CEW complex holds efficient NIR-II emission of 1,000–1,400 nm via endogenous H_2S-induced *in situ* chemical reaction to form Ag_2S quantum dots (QDs). After reaction, the designed Ag-CEW complex with high photo-stability and biocompatibility was successfully used for NIR-II imaging-guided specific visualization and precise location of colorectal cancer via endogenous H_2S activation. Therefore, our findings provide a new route for specifically targeting diagnosis of colon cancer based on the *in situ*-activatable NIR-II probe.

INTRODUCTION

Among adults older than 50 years, colorectal cancer incidence rates had increased by 22% from 2000 to 2013, which was one of the most common malignancies in the world (Siegel et al., 2017; Ricci-Vitiani et al., 2006). Also, some clinical diagnostic methods for colorectal cancer such as colonoscopy, surgical procedures, and carcinoembryonic antigen are well explored (Hassan and Repici, 2017; Zhang et al., 2017a, 2017b; Xu et al., 2018; An et al., 2018). However, all these traditional methods still suffer from some inevitable drawbacks, including extensive medical experience needed, low sensitivity, and great pain to patients (Hassan and Repici, 2017; Zhang et al., 2017a, 2017b; Xu et al., 2018; An et al., 2018). Therefore the development of a non-invasive early diagnostic technique with high sensitivity is urgently demanded for specific visualization of colorectal cancer.

Optical imaging method capable of providing direct visualization of disease with high spatial/temporal resolution and high sensitivity has emerged as an indispensable tool for non-invasive disease diagnosis (Ellenbroek and van Rheenen, 2014; Yang and Yuste, 2017; He et al., 2018; Zhao et al., 2016). Differing from conventional optical imaging by using the visible and first near-infrared (NIR-I, 700–900 nm) regions, second NIR (NIR-II) optical imaging with emission ranging from 1,000 to 1,700 nm is considered as the next-generation advanced optical imaging technique with superior imaging sensitivity and significant improvement in spatial resolution owing to the remarkably reduced scattering losses (Hong et al., 2012a, 2012b, 2014a, 2014b; Naczynski et al., 2013; Dang et al., 2016; Zhao et al., 2018). *In vivo* NIR-II imaging began with the utilization of single-walled carbon nanotubes (Hong et al., 2014a, 2014b, 2015; Diao et al., 2015); since then, several other probes including small-molecule dyes (Yang et al., 2018), semiconductor quantum dots (Bruns et al., 2017; Hong et al., 2012a, 2012b), and rare-earth-doped materials (Zhong et al., 2017; Li et al., 2018, 2019; Xue et al., 2018) have been explored for *in vivo* NIR-II imaging. However, most of the developed NIR-II probes presented low specificity for tumor diagnosis, resulting in the absence of targeting visualization of colorectal cancer. Therefore the development of probe with high sensitivity, excellent spatial resolution, and tumor-targeted properties holds great significance for improving the diagnostic sensitivity.

It is well known that colon cancer cells overexpress cystathionine-β-synthase, resulting in larger amounts of H_2S in tumor than the adjacent normal tissue or non-transformed cells (Szabo et al., 2013). Various fluorescent probes for H_2S intracellular imaging were successfully developed by using the visible and NIR-I region (Lin et al., 2015; Yu et al., 2014; Wang et al., 2013a, 2013b, 2018, 2019; Shi et al., 2017; Zhang et al., 2017a,

[1]School of Physics and Electronics and Key Laboratory of Low-dimensional Quantum Structures and Quantum Control of the Ministry of Education, Synergetic Innovation Center for Quantum Effects and Applications, Hunan Normal University, Changsha, Hunan 410081, China

[2]Department of Applied Physics, The Hong Kong Polytechnic University, Hong Kong, China

[3]Lead Contact

*Correspondence: songjunz@hunnu.edu.cn (S.Z.), jh.hao@polyu.edu.hk (J.H.)

https://doi.org/10.1016/j.isci.2019.06.034

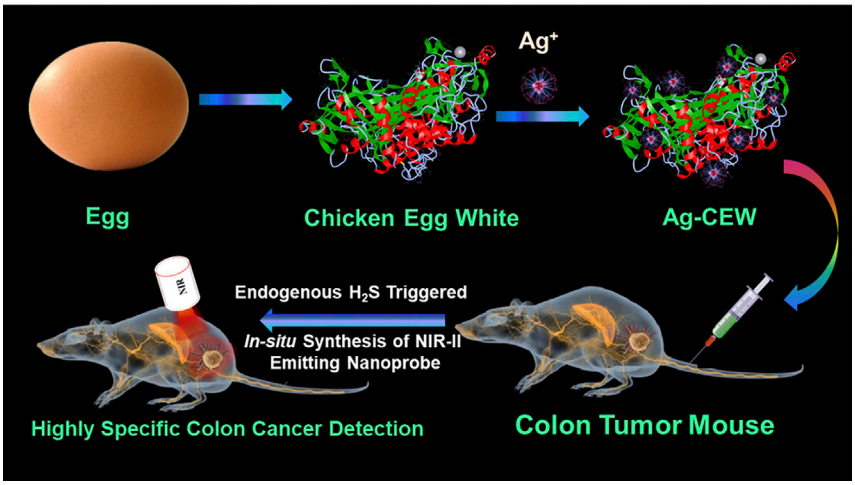

Scheme 1. Schematic Illustration of the Synthesis Procedure of Ag-CEW Complex and Endogenous H_2S-Triggered *In Situ* Synthesis of Ag_2S QDs from Ag-CEW Complex for Highly Specific Visualization of Colon Cancer

2017b). However, few probes have been employed for *in vivo* H_2S-stimulated imaging owing to the limitations of penetration depth and poor spatial resolution by using the traditional visible and NIR-I optical imaging (Lin et al., 2015; Yu et al., 2014; Wang et al., 2013a, 2013b). Undoubtedly, H_2S-activated emissions in NIR-II window can provide valuable insight into the accurate and specific diagnosis of colorectal cancers *in vivo*. Nevertheless, *in situ* endogenous H_2S-activated NIR-II-emissive probes for targeting diagnosis of colon cancer was still scarcely explored. Very recently, a conceptual study was proposed by designing an H_2S-activated NIR-II optical probe based on the core-shell silica nanocomposites encapsulating an H_2S-responsive organic molecule for detection of colon cancer *in vivo* (Xu et al., 2018). However, this NIR-II fluorescence imaging probe suffers from some intrinsic problems, such as the complex synthesis process, photo-bleaching, and low photo-stability of organic molecular probes, which impede its further applications in bioimaging fields (He et al., 2018; Shi et al., 2018). Therefore, developing a new H_2S-activated inorganic nanoparticulate probe with highly simple synthesis method, non-photobleaching nature, high quantum yield (QY), and high photo-stability is highly desirable.

Biomolecule-assisted synthesis (Zhou et al., 2015; Dickerson et al., 2008; Wang et al., 2013a, 2013b; Chen et al., 2015a, 2015b, 2015c; Gao et al., 2014) has been demonstrated to be an excellent and useful method for the preparation of inorganic nanomaterials with good biocompatibility and stability in biomedical applications. For example, bovine serum albumin (BSA), tryptophan-based peptides, and chicken egg white (CEW) have been used to prepare carbon-, noble metal-, and metal-based oxide or sulfide nanomaterials (Chong et al., 2015; Wang et al., 2012, 2015; Chen et al., 2015a, 2015b; Reithofer et al., 2014; Zhang et al., 2014; Jana et al., 2014). Among these biomolecules, the CEW complex consists of multiple proteins and is extremely cheap and easily available in daily life (Zhou et al., 2015; Dickerson et al., 2008). Thus, exploring new H_2S-activatable NIR-II probe via CEW complex is highly desirable for specific colon cancer detection.

Herein, endogenous H_2S-triggered NIR-II-emitting nanoprobe based on Ag-CEW complex (Scheme 1) for specific visualization of colorectal cancer was designed via *in situ* chemical reaction between Ag-CEW and overexpressed H_2S gas in colorectal cancer. The Ag-CEW complex was synthesized by an environment-friendly method by using CEW as the surface ligands for chelating Ag^+ at room temperature. More importantly, *in situ* H_2S-activatable NIR-II-emitting nanoprobe for *in vivo* specific diagnosis of colorectal cancer was achieved. *In vivo* histological examination was carried out to evaluate the biotoxicity of the Ag-CEW complex.

RESULTS

Preparation and Characterization of the Ag-CEW Complex after Adding S^{2-}

As a proof of concept, Na_2S was used to simulate endogenous H_2S for investigating the *in situ* reaction of Ag-CEW complex with S^{2-}. As shown in Figure 1A, when Ag^+ (1 mmol) is added into CEW aqueous solution

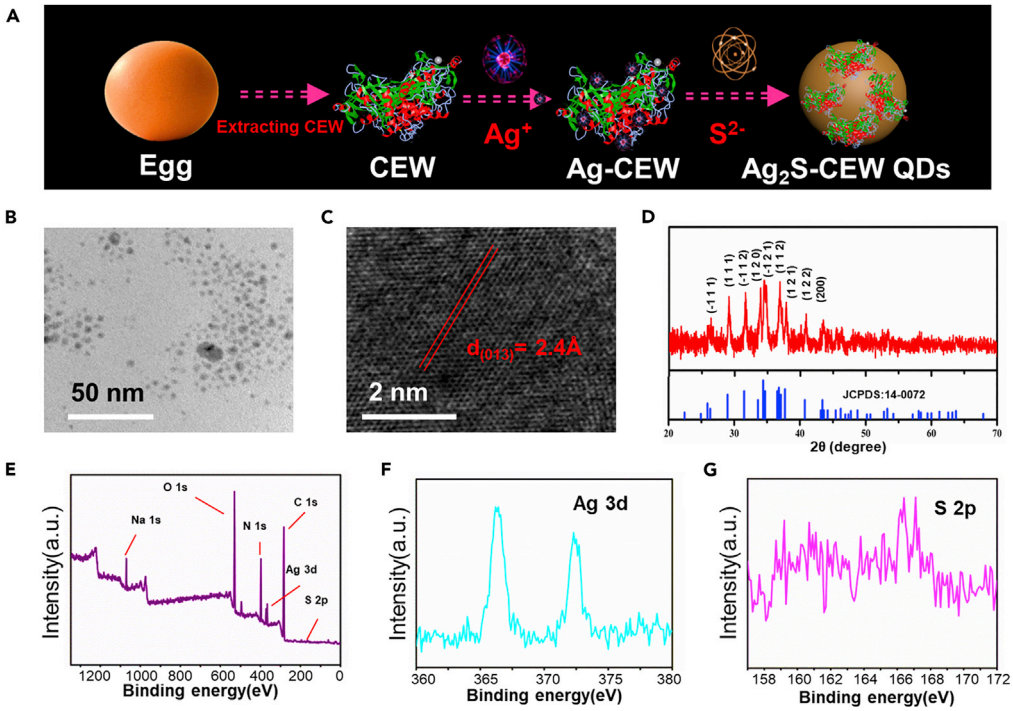

Figure 1. Microstructure and Crystal Phase of the As-Prepared Ag_2S-CEW QDs

(A) Schematic illustration of the Na_2S-triggered *in situ* chemical reaction with Ag-CEW to form Ag_2S QDs.

(B) TEM image of Ag_2S-CEW QDs.

(C) High-resolution TEM image of Ag_2S-CEW QDs.

(D) The typical XRD pattern of the *in situ*-synthesized Ag_2S-CEW QDs.

(E) XPS spectrum for Ag_2S-CEW QDs.

(F) The corresponding high-resolution XPS spectrum of Ag (3d).

(G) The corresponding high-resolution XPS spectrum of S (2P).

(2 mL), CEW can adsorb Ag^+ ions and generate Ag-CEW complex. After adding Na_2S aqueous solution, Ag^+ embedded in the three-dimensional structures of the CEW proteins could react with S^{2-} at room temperature within 200 ms (Figure S1) to produce Ag_2S quantum dots (QDs). The shape and size of the CEW-capped Ag_2S QDs were characterized by transmission electron microscopy (TEM). As demonstrated in Figure 1B, CEW-capped Ag_2S QDs present ultrasmall particle structure with size of about 6.5 nm. High-resolution TEM (Figure 1C) revealed the high crystallization nature of Ag_2S QDs, and the distance between the lattice fringes was measured to be 2.4 Å, corresponding to the d-spacing of the (013) crystal plane of the monoclinic phase. The crystal phase structure was further detected by X-ray diffraction (Figure 1D), in which all the diffraction peaks were matched well with the standard monoclinic phase Ag_2S (JCPDS File No. 14-0072). Furthermore, the elemental compositions of Ag_2S QDs were investigated by X-ray photoelectron spectroscopy (XPS). As demonstrated in Figure 1E, the sample is mainly composed of Ag, S, C, O, N, and Na elements. And the XPS peaks at 367.7 and 373.7 eV are related to the Ag $3d_{5/2}$ and $3d_{3/2}$, respectively. In contrast, the $S2_p$ peak at 162.8 eV is ascribed to S in Ag_2S-CEW QDs (Figures 1F and 1G), further verifying the formation of Ag_2S. All these results demonstrated that Ag_2S QDs were readily achieved by adding Na_2S via chemical reaction with Ag-CEW complex at room temperature. To prove the capability of CEW coordination with other metallic ions as a general synthesis strategy, Pb-CEW complex was also synthesized by the same method as the Ag-CEW complex. After adding Na_2S, CEW-capped PbS QDs (Figures S2 and S3) were also obtained. These findings reveal that our designed biomolecule-assisted synthesis strategy is a general route for ultrafast formation of sulfide-based QDs at room temperature without heating.

NIR-II Optical Characteristics of Ag-CEW Complex

Owing to the efficient NIR-II emission of Ag_2S (Du et al., 2010; Li et al., 2015), the S^{2-} activated NIR-II emission properties of Ag-CEW complex were then studied. The Ag-CEW complex presents significant

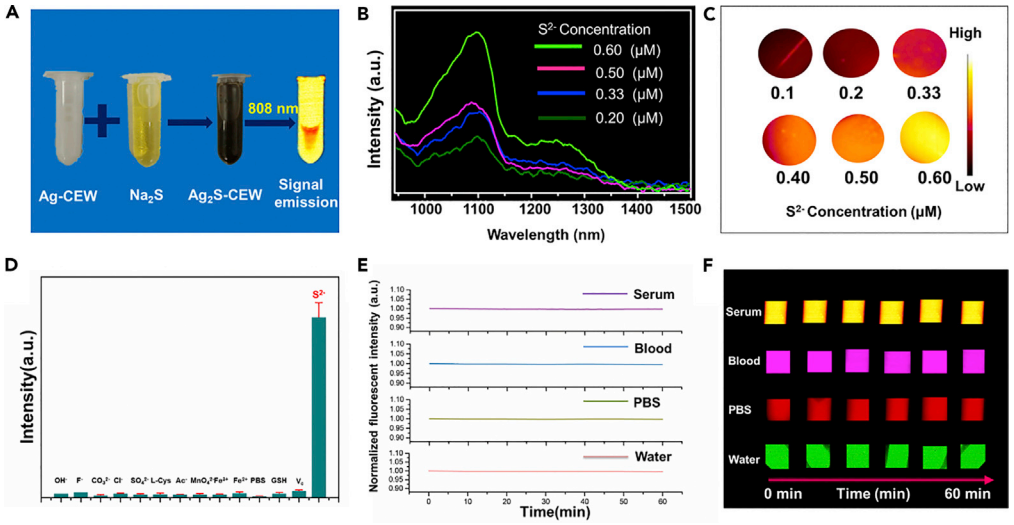

Figure 2. NIR-II Luminescence Properties of Ag-CEW after Adding Na_2S

(A) Schematic illustration of S^{2-}-triggered NIR-II emission in Ag-CEW solution.

(B) S^{2-} concentration-dependent NIR-II emission spectra of Ag-CEW in the presence of Na_2S under 808 nm laser excitation.

(C) *In vitro* NIR-II phantom imaging of Ag-CEW solutions by adding different concentrations of Na_2S.

(D) The NIR-II signal intensity of Ag-CEW solutions treated with different electrolytes and biomolecules, exhibiting highly specific response to S^{2-}.

(E) The photo-stability curve in serum, blood, phosphate-buffered saline (PBS), and water.

(F) *In vitro* phantom NIR-II fluorescent imaging of the Ag_2S-CEW QDs in different media (serum, blood, PBS, and water) at the same concentration under continuous 808 nm laser illumination.

optical response to Na_2S (Figure 2A). After adding Na_2S solution, the UV-visible absorption spectrum of the Ag-CEW complex solution showed an increasing absorption in the shorter wavelengths (Figure S4), which was consistent with previously reported Ag_2S QDs, indicating the formation of Ag_2S-CEW QDs (Du et al., 2010; Li et al., 2015). Then the fluorescent emission spectra (Figure 2B) of Ag_2S-CEW QDs were detected, demonstrating a strong NIR-II emission peak around 1,090 nm. As demonstrated in Figure 2B, with increasing the S^{2-} concentration from 0.10 to 0.60 μM, the NIR-II emission intensity is gradually increased, which is also vividly revealed by *in vitro* phantom imaging (Figure 2C). Also, the QY of the NIR-II emission in the explored Ag_2S-CEW QDs dispersed in water is measured to be ~11%, which is higher than that of organic small-molecule probes (Yang et al., 2018). To further reveal the size-dependent NIR-II emission, Ag_2S-CEW QDs with different sizes by using the same method were synthesized. As demonstrated in Figure S5, with increasing particle size, the NIR-II emitting intensity was dramatically decreased, which was consistent with previous report (Zhang et al., 2012).

It is well known that H_2S plays an important role in colon cancer with concentrations ranging from 0.3 to 3.4 mmol L^{-1} (Szabo et al., 2013; Hellmich and Szabo, 2015; Chen et al., 2013). Therefore, highly sensitive and specific detection of S^{2-} is required. To demonstrate the detection limit, the quantitative emission intensity (Figure S6) and linear relationship (Figure S7) within concentration ranging from 0.10 to 0.60 μM of S^{2-} were studied, indicating the ultrasensitive detection of S^{2-} with detectable limit of 35 nM, which was more accurate for H_2S detection than the previously reported fluorescent H_2S probes (Lin and Chang, 2012). Therefore the detection limit of Ag-CEW is sufficient for detection of colon cancer *in vivo*. To further reveal the specific detection of S^{2-}, various ions and biomolecules were used for NIR-II luminescence response (Figure 2D). As demonstrated, unlike the notable optical response observed in the presence of S^{2-}, no variations in fluorescence intensity were observed upon the addition of the same concentration of other molecules. These findings demonstrate that the Ag-CEW complex can be used as a highly sensitive and specific probe for colon cancer detection owing to the overexpression of H_2S in tumor site.

As a comparison study, the Ag-BSA complex and $AgNO_3$ solutions with same concentration were also used for S^{2-}-induced NIR-II emission. As shown in Figure S8, Ag-CEW complex presents higher NIR-II emission

intensity than Ag-BSA and $AgNO_3$, which is mainly attributed to the small size of Ag_2S QDs (Figure S9) synthesized by using Ag-CEW complex. Thus the Ag-CEW complex is more beneficial for NIR-II optical bioimaging applications than Ag-BSA and $AgNO_3$. Moreover, the photo-stability curve (Figure 2E) and *in vitro* phantom bioimaging (Figure 2F) in different buffer solutions reveal that the Ag_2S-CEW QDs formed by *in situ* reaction present superior photo-stability with a photo-bleaching degree of 0.6% in 60 min, which is relatively lower than the organic molecule dye (Hong et al., 2014a, 2014b).

To further prove the binding stability of Ag and CEW molecules, the leaked amounts of Ag^+ in Ag-CEW complex and $AgNO_3$ were also measured by using a silver assay kit as direct color indicator. As shown in Figure S10, free Ag^+ at a low concentration of about 0.00–4.60 nM and pH value ranging from 4 to 7 can react with the silver assay kit to change the solution color from transparent to red color. In contrast, the Ag-CEW complex solution presents no obvious color change even at a concentration ranging from 0.46 nM to 4.6 nM, demonstrating the strong chelation of Ag^+ and CEW and high structure stability of Ag-CEW complex. These results reveal no leakage of Ag^+ or very limited leakage less than about 0.46 nM from the Ag-CEW complex, which is significantly lower than the safe level of free Ag^+ of 9.2 nM (Greulich et al., 2012; Chernousova and Epple, 2013).

NIR-II Optical Imaging-Guided Specific Diagnosis of Colorectal Tumor

Before *in vivo* imaging, *in vitro* cell imaging was first performed. The HCT-116 cells were incubated with Ag-CEW complex for 36 h at 37°C. The fluorescent images of cells were recorded by using the homemade NIR-II imaging system under irradiation at 808 nm laser. Compared with the control group (Figure S11A) treated with PBS, a bright NIR-II fluorescence signal (Figure S11B) was observed from HCT-116 cells cultured with Ag-CEW complex, validating the H_2S (generated from HCT-116 cells)-activated NIR-II emission *in vitro*.

Encouraged by the S^{2-}-activated high-performance NIR-II emission of Ag-CEW complex, *in vivo in situ* reaction of Ag-CEW complex with endogenous H_2S in colon cancer was carried out. For specifically lighting up colon cancer, tumor-bearing (HCT116) mouse was injected with Ag-CEW complex solution and used for *in vivo* NIR-II fluorescence imaging. Owing to the large overexpressed levels of endogenous H_2S, a significant NIR-II signal (Figure 3A) was only observed in tumor site and gradually increased by prolonging time. After 5 days of injection, the NIR-II signal reached up to a maximum value, indicating the complete *in situ* chemical reaction between Ag-CEW and endogenous H_2S to form NIR-II-emitting Ag_2S QDs. In addition, the signal-to-noise ratio (SNR) between the tumor and normal site was further evaluated to be 32, verifying the highly sensitive optical diagnosis of colon tumor. To further demonstrate the specific recognition of colon cancer, a lung (A549) tumor-bearing model was also used for NIR-II optical imaging. As shown in Figure 3B, almost no NIR-II signal was observed before injection of Na_2S (1 μM) in lung cancer. In contrast, with injection of Na_2S after 7 days, the tumor site also presents a bright NIR-II signal. The corresponding NIR-II average intensity of HCT116/A549 tumor-bearing mice was exhibited in Figure 3C. The specific and precise location of NIR-II optical signals in colon tumor revealed that the Ag-CEW complex could specifically light up colorectal cancer. Moreover, the inductively coupled plasma mass spectrometry analysis (Figure S12) reveals the presence of Ag and S ions, further demonstrating that the NIR-II emission in tumor tissues originated from *in situ* endogenous H_2S-activatable Ag_2S QDs.

It should be noted that most of the developed NIR-II probes presented low specificity for tumor diagnosis and undesired background interference signals from the reticuloendothelial (RES) system, such as the liver and spleen (Hong et al., 2012a, 2012b; Hu et al., 2015, Xue et al., 2018; Li et al., 2019). Moreover, it is still a great challenge to design an inorganic probe for highly specific tumor diagnosis with eliminated unspecific interference signal from the RES system (liver, spleen). In our designed endogenous H_2S-activated Ag-CEW system, the unspecific signal from normal RES tissues can be completely eliminated because of the absence of overexpressed H_2S in these tissues. To reveal this, *ex vivo* imaging (Figure S13) of the isolated organs such as the heart, liver, spleen, lung, and kidney was performed and no NIR-II signals were observed in these organs, validating the successful elimination of the interference signal from the RES system. Therefore, compared with the direct injection of Ag_2S QDs (Hong et al., 2012a, 2012b; Hu et al., 2015), our designed endogenous H_2S-activated Ag-CEW probes not only present much higher SNR (>30) but also hold highly specific imaging of colorectal tumor with eliminated unspecific interference signal from the RES system. Therefore the designed Ag-CEW complex can be used as ideal endogenous H_2S-triggered NIR-II emitting probe for highly specific and sensitive diagnosis of colon cancer.

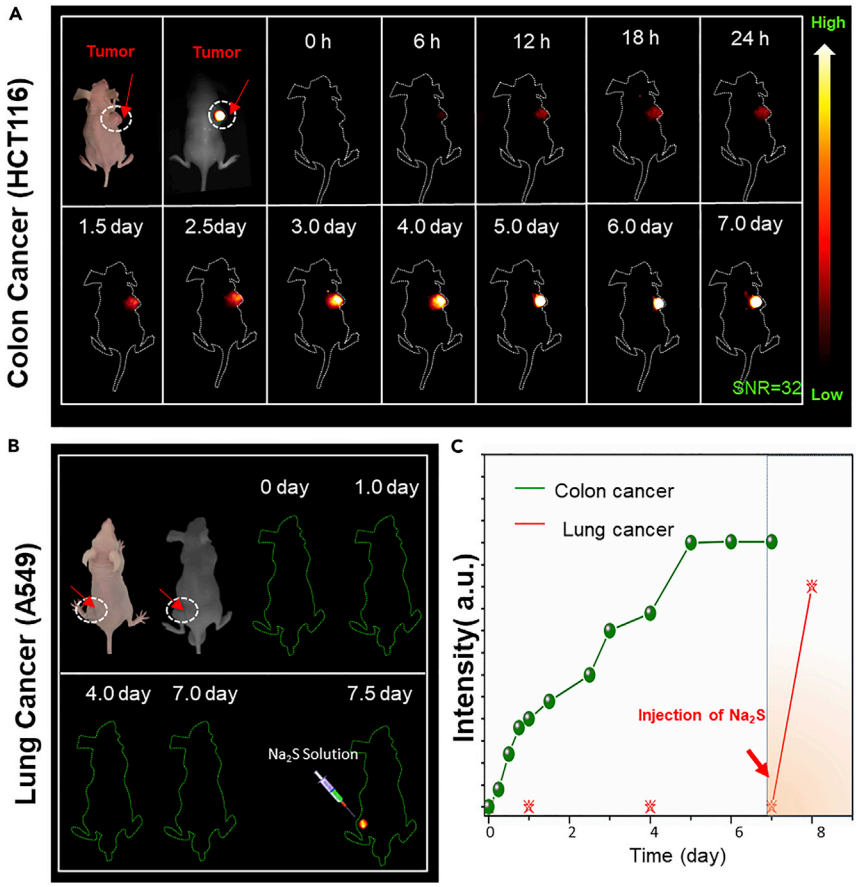

Figure 3. *In Vivo*-Specific Visualization of Colon Cancer Based on *In Situ* Endogenous H_2S Activation of Ag-CEW Complex

(A) Colon (HCT116) tumor-bearing mouse.

(B) Lung (A549) tumor-bearing mouse.

(C) The mean NIR-II signal intensity change in the tumor region from 1 to 7 days.

To detect the pathological changes induced by the Ag-CEW complex, a histological examination of the mouse organs was performed. As shown in Figure S14, no noticeable organ damage was found in the stained tissues after intravenous injection of Ag-CEW from 7 to 30 days, validating the negligible biotoxicity and high biocompatibility of Ag-CEW complex *in vivo*.

DISCUSSION

In summary, we explore an *in situ* endogenous H_2S-activatable NIR-II-emissive Ag-CEW nanoprobe for intelligently lighting up colorectal cancer. Our designed Ag-CEW complex possesses high photo-stability and NIR-II emission at 1,090 nm. *In vivo* toxicity tests revealed the excellent biocompatibility and negligible side effects of the Ag-CEW complex. Importantly, the Ag-CEW complex was successfully used for NIR-II optical imaging-guided specific diagnosis of colorectal tumor with high sensitivity and completely eliminated interference signal from RES system by *in situ* H_2S activation. Therefore, it is expected that our designed endogenous H_2S-triggered NIR-II emitting probe can facilitate the development of specific diagnosis technique for *in vivo* colon cancer detection.

Limitations of Study

We have designed *in situ* endogenous H_2S-activatable NIR-II-emissive Ag-CEW nanoprobe for intelligently lighting up colorectal cancer. Cell types of colon cancer, including HT-29 and COLO3, have not been detected and are worth investigating in the future.

METHODS

All methods can be found in the accompanying Transparent Methods supplemental file.

SUPPLEMENTAL INFORMATION

Supplemental Information can be found online at https://doi.org/10.1016/j.isci.2019.06.034.

ACKNOWLEDGMENTS

This work was supported by National Natural Science Foundation of China (No. 21671064), Science and Technology Planning Project of Hunan Province (No. 2017RS3031), and Natural Science Foundation of Hunan Province, China (No. 2019JJ10002).

AUTHOR CONTRIBUTIONS

S.Z. conceived and designed the experiments. S.Z. and J.H. supervised the research. Z.D. carried out the experiments and characterizations. M.J., Y.L., and H.L. analyzed the data and co-wrote the manuscript.

DECLARATION OF INTERESTS

The authors declare no competing interests.

Received: February 25, 2019
Revised: May 28, 2019
Accepted: June 22, 2019
Published: July 26, 2019

REFERENCES

An, L., Wang, X.D., Rui, X.C., Lin, J.M., Yang, H., Tian, Q.W., Tao, C., and Yang, S.P. (2018). The in situ sulfidation of Cu_2O by endogenous H_2S for colon cancer theranostics. Angew. Chem. Int. Ed. *2018*, 15782–15786.

Bruns, O.T., Bischof, T.S., Harris, D.K., Franke, D., Shi, Y., Riedemann, L., Bartelt, A., Jaworski, F.B., Carr, J.A., Rowlands, C.J., et al. (2017). Next-generation *in vivo* optical imaging with short-wave infrared quantum dots. Nat. Biomed. Eng. *1*, 0056.

Chen, D.H., Zhao, C.Q., Ye, J., Li, Q.W., Liu, X.L., Su, M.N., Jiang, H., Amatore, C., Selke, M., and Wang, X.M. (2015a). *In situ* biosynthesis of fluorescent platinum nanoclusters: toward self-bioimaging-guided cancer theranostics. ACS Appl. Mater. Interfaces *7*, 18163–18169.

Chen, Q., Liang, C., Wang, C., and Liu, Z. (2015b). An imagable and photothermal "Abraxane-Like" nanodrug for combination cancer therapy to treat subcutaneous and metastatic breast tumors. Adv. Mater. *27*, 903–910.

Chen, Q., Wang, X., Wang, C., Feng, L.Z., Li, Y.G., and Liu, Z. (2015c). Drug-induced self-assembly of modified albumins as nano-theranostics for tumor-targeted combination therapy. ACS Nano *9*, 5223–5233.

Chernousova, S., and Epple, M. (2013). Silver as antibacterial agent: ion, nanoparticle, and metal. Angew. Chem. Int. Ed. *52*, 1636–1653.

Chong, Y., Ge, C.C., Yang, Z.X., Garate, J.A., Gu, Z.L., Weber, J.K., Liu, J.J., and Zhou, R.H. (2015). Reduced cytotoxicity of graphene nanosheets mediated by blood-protein coating. ACS Nano *9*, 5713–5724.

Chen, Y.C., Zhu, C.C., Yang, Z.H., Chen, J.J., He, Y.F., Jiao, Y., He, W.J., Qiu, L., Cen, J.J., and Guo, Z.J. (2013). A ratiometric fluorescent probe for rapid detection of hydrogen sulfide in mitochondria. Angew. Chem. Int. Ed. *52*, 1688–1691.

Dang, X., Gu, L., Qi, J., Correa, S., Zhang, G., Belcher, A.M., and Hammond, P.T. (2016). Layer-by-layer assembled fluorescent probes in the second near-infrared window for systemic delivery and detection of ovarian cancer. Proc. Natl. Acad. Sci. U S A *113*, 5179–5184.

Diao, S., Hong, G.S., Antaris, A.L., Blackburn, J.L., Cheng, K., Cheng, Z., and Dai, H.J. (2015). Biological imaging without autofluorescence in the second near-infrared region. Nano Res. *8*, 3027–3034.

Dickerson, M.B., Sandhage, K.H., and Naik, R.R. (2008). Protein- and peptide-directed syntheses of inorganic materials. Chem. Rev. *108*, 4935–4978.

Du, Y.P., Xu, B., Fu, T., Cai, M., Li, F., Zhang, Y., and Wang, Q.B. (2010). Near-infrared photoluminescent Ag_2S quantum dots from a single source precursor. J. Am. Chem. Soc. *132*, 1470–1471.

Ellenbroek, S.I.J., and van Rheenen, J. (2014). Imaging hallmarks of cancer in living mice. Nat. Rev. Cancer *14*, 406–418.

Greulich, C., Braun, D., Peetsch, A., Diendorf, J., Siebers, B., Epple, M., and Koller, M. (2012). The toxic effect of silver ions and silver nanoparticles towards bacteria and human cells occurs in the same concentration range. RSC Adv. *2*, 6981–6987.

Gao, S.P., Chen, D.H., Li, Q.W., Ye, J., Jiang, H., Amatore, C., and Wang, X.M. (2014). Near-infrared fluorescence imaging of cancer cells and tumors through specific biosynthesis of silver nanoclusters. Sci. Rep. *4*, 4384.

Hassan, C., and Repici, A. (2017). Recent advances in diagnostic colonoscopy for colorectal cancer screening. Am. J. Roentgenol. *209*, 88–93.

He, S.Q., Song, J., Qu, J.L., and Cheng, Z. (2018). Crucial breakthrough of second near-infrared biological window fluorophores: design and synthesis toward multimodal imaging and theranostics. Chem. Soc. Rev. *47*, 4258–4278.

Hellmich, M.R., and Szabo, C. (2015). Hydrogen sulfide and cancer. Handb. Exp. Pharmacol. *230*, 233–241.

Hong, G.S., Lee, J.C., Robinson, J.T., Raaz, U., Xie, L.M., Huang, J.P., Cooke, N.F., and Dai, H.J. (2012a). Multifunctional *in vivo* vascular imaging using near-infrared II fluorescence. Nat. Med. *18*, 1841–1846.

Hong, G.S., Robinson, J.T., Zhang, Y.J., Diao, S., Antaris, A.L., Wang, Q.B., and Dai, H.J. (2012b). *In vivo* fluorescence imaging with Ag_2S quantum dots in the second near-infrared region. Angew. Chem. Int. Ed. *51*, 9818–9821.

Hong, G.S., Diao, S., Chang, J.L., Antaris, A.L., Chen, C.X., Zhang, B., Zhao, S., Atochin, D.N., Huang, P.L., Andreasson, K.I., et al. (2014a). Through-skull fluorescence imaging of the brain in a new near-infrared window. Nat. Photonics *8*, 723–730.

Hong, G.S., Zou, Y., Antaris, A.L., Diao, S., Wu, D., Cheng, K., Zhang, X., Chen, C., Liu, B., He, Y.,

et al. (2014b). Ultrafast fluorescence imaging *in vivo* with conjugated polymer fluorophores in the second near-infrared window. Nat. Commun. *5*, 4206.

Hong, G.S., Diao, S., Antaris, A.L., and Dai, H.J. (2015). Carbon nanomaterials for biological imaging and nanomedicinal therapy. Chem. Rev. *115*, 10816–10906.

Hu, F., Li, C.Y., Zhang, Y.J., Wang, M., Wu, D.M., and Wang, Q.B. (2015). Real-time *in vivo* visualization of tumor therapy by a near-infrared-II Ag_2S quantum dot-based theranostic nanoplatform. Nano Res. *8*, 1637–1647.

Jana, S., Manna, S., Nayak, A.K., Sen, K.K., and Basu, S.K. (2014). Carbopol gel containing chitosan-egg albumin nanoparticles for transdermal aceclofenac delivery. Colloids Surf. B *114*, 36–44.

Li, C.Y., Li, F., Zhang, Y.J., Zhang, W.J., Zhang, X.E., and Wang, Q.B. (2015). Real-Time monitoring surface chemistry-dependent *in vivo* behaviors of protein nanocages via encapsulating an NIR-II Ag_2S quantum dot. ACS Nano *9*, 12255–12263.

Li, Y.B., Li, X.L., Xue, Z.L., Jiang, M.Y., Zeng, S.J., and Hao, J.H. (2018). Second near-infrared emissive lanthanide complex for fast renal-clearable in vivo optical bioimaging and tiny tumor detection. Biomaterials *169*, 35–44.

Li, Y.B., Zeng, S.J., and Hao, J.H. (2019). Non-invasive optical guided tumor metastasis/vessel imaging by using lanthanide nanoprobe with enhanced down-shifting emission beyond 1500 nm. ACS Nano *13*, 248–259.

Lin, V.S., and Chang, C.J. (2012). Fluorescent probes for sensing and imaging biological hydrogen sulfide. Curr. Opin. Chem. Biol. *16*, 595–601.

Lin, V.S., Chen, W., Xian, M., and Chang, C.J. (2015). Chemical probes for molecular imaging and detection of hydrogen sulfide and reactive sulfur species in biological systems. Chem. Soc. Rev. *44*, 4596–4618.

Naczynski, D., Tan, M., Zevon, M., Wall, B., Kohl, J., Kulesa, A., Chen, S., Roth, C., Riman, R., and Moghe, P. (2013). Rare-earth-doped biological composites as *in vivo* shortwave infrared reporters. Nat. Commun. *4*, 2199.

Reithofer, M.R., Lakshmanan, A., Ping, A.T.K., Chin, J.M., and Hauser, C.A.E. (2014). In situ synthesis of size-controlled, stable silver nanoparticles within ultrashort peptide hydrogels and their anti-bacterial properties. Biomaterials *35*, 7535–7542.

Ricci-Vitiani, L., Lombardi, D.G., Pilozzi, E., Biffoni, M., Todaro, M., Peschle, C., and De Maria, R. (2006). Identification and expansion of human colon-cancer-initiating cells. Nature *445*, 111–115.

Shi, B., Gu, X.F., Fei, Q., and Zhao, C.C. (2017). Photoacoustic probes for real-time tracking of endogenous H_2S in living mice. Chem. Sci. *8*, 2150–2155.

Shi, B., Yan, Q.L., Tang, J., Xin, K., Zhang, J.C., Zhu, Y., Xu, G., Wang, R.C., Chen, J., Gao, W., et al. (2018). Hydrogen sulfide-activatable second near-infrared fluorescent nanoassemblies for targeted photothermal cancer therapy. Nano Lett. *18*, 6411–6416.

Szabo, C., Coletta, C., Chao, M.K., Szczesny, B., Papapetropoulos, A., and Hellmich, M.R. (2013). Tumor-derived hydrogen sulfide, produced by cystathionine-β-synthase, stimulates bioenergetics, cell proliferation, and angiogenesis in colon cancer. Proc. Natl. Acad. Sci. U S A *110*, 12474–12479.

Siegel, R.L., Miller, K.D., Fedewa, S.A., Ahnen, D.J., Meester, R.G.S., Barzi, A., and Jemal, A. (2017). Colorectal cancer statistics. CA Cancer J. Clin. *67*, 177–193.

Wang, F.Y., Xu, G., Gu, X.F., Wang, Z.J., Wang, Z.Q., Shi, B., Lu, C.F., Gong, X.Q., and Zhao, X.X. (2018). Realizing highly chemoselective detection of H_2S *in vitro* and *in vivo* with fluorescent probes inside core-shell silica nanoparticles. Biomaterials *159*, 82–90.

Wang, J., Wang, C.F., and Chen, S. (2012). Amphiphilic egg-derived carbon dots: rapid plasma fabrication, pyrolysis process, and multicolor printing patterns. Angew. Chem. Int. Ed. *51*, 9297–9301.

Wang, J.L., Lin, W.Y., and Li, W.L. (2013a). Three-channel fluorescent sensing via organic white light-emitting dyes for detection of hydrogen sulfide in living cells. Biomaterials *34*, 7429–7436.

Wang, J.L., Zhang, G., Li, Q.W., Jiang, H., Liu, C.Y., Amatore, C., and Wang, X.M. (2013b). *In vivo* self-bio-imaging of tumors through *in situ* biosynthesized fluorescent gold nanoclusters. Sci. Rep. *3*, 1157.

Wang, R.C., Dong, K.K., Xu, G., Shi, B., Zhu, T., Shi, P., Guo, Z.Q., Zhu, W.H., and Zhao, C.C. (2019). Activatable near-infrared emission-guided on-demand administration of photodynamic anticancer therapy with a theranostic nanoprobe. Chem. Sci. *10*, 2785.

Wang, Y., Yang, T., Ke, H.T., Zhu, A.J., Wang, Y.J., Wang, J.X., Shen, J.K., Liu, G., Chen, C.Y., Zhao, Y.L., and Chen, H.B. (2015). Smart albumin-biomineralized nanocomposites for multimodal imaging and photothermal tumor ablation. Adv. Mater. *27*, 3874–3882.

Xu, G., Yan, Q., Lv, X., Zhu, Y., Xin, K., Shi, B., Wang, R., Chen, J., Gao, W., Shi, P., et al. (2018). Imaging of colorectal cancers using activatable nanoprobes with second near-infrared window emission. Angew. Chem. Int. Ed. *57*, 3626–3630.

Xue, Z.L., Zeng, S.J., and Hao, J.H. (2018). Non-invasive through-skull brain vascular imaging and small tumor diagnosis based on NIR-II emissive lanthanide nanoprobes beyond 1500 nm. Biomaterials *171*, 153–163.

Yang, Q., Hu, Z., Zhu, S., Ma, R., Ma, H., Ma, Z., Wan, H., Zhu, T., Jiang, Z., Liu, W., et al. (2018). Donor engineering for NIR-II molecular fluorophores with enhanced fluorescent performance. J. Am. Chem. Soc. *140*, 1715–1724.

Yang, W., and Yuste, R. (2017). *In vivo* imaging of neural activity. Nat. Methods *14*, 349–359.

Yu, F.B., Han, X.Y., and Chen, L.X. (2014). Fluorescent probes for hydrogen sulfide detection and bioimaging. Chem. Commun. (Camb.) *50*, 12234–12249.

Zhao, J.Y., Chen, G., Gu, Y.P., Cui, R., Zhang, Z.L., Yu, Z.L., Tang, B., Zhao, Y.F., and Pang, D.W. (2016). Ultrasmall magnetically engineered Ag_2Se quantum dots for instant efficient labeling and whole-body high-resolution multimodal real-time tracking of cell-derived microvesicles. J. Am. Chem. Soc. *138*, 1893–1903.

Zhao, J.Y., Zhong, D., and Zhou, S.B. (2018). NIR-I-to-NIR-II fluorescent nanomaterials for biomedical imaging and cancer therapy. J. Mater. Chem. B *6*, 349–365.

Zhang, Y., Hong, G.S., Zhang, Y.J., Chen, G.C., Li, F., Dai, H.J., and Wang, Q.B. (2012). Ag_2S quantum dot: a bright and biocompatible fluorescent nanoprobe in the second near-infrared window. ACS Nano *6*, 3695–3702.

Zhang, K., Zhang, J., Xi, Z., Li, L.Y., Gu, X.X., Zhang, Q.Z., and Yi, L. (2017a). A new H_2S-specific near-infrared fluorescence-enhanced probe that can visualize the H_2S level in colorectal cancer cells in mice. Chem. Sci. *8*, 2776–2781.

Zhang, Y., Chen, Z., and Li, J. (2017b). The current status of treatment for colorectal cancer in China. Medicine *96*, e8242.

Zhang, X.D., Luo, Z.T., Chen, J., Shen, X., Song, S., Sun, Y., Fan, S., Fan, F., Leong, D.T., and Xie, J.P. (2014). Ultrasmall $Au_{10-12}(SG)_{10-12}$ nanomolecules for high tumor specificity and cancer radiotherapy. Adv. Mater. *26*, 4565–4568.

Zhong, Y., Ma, Z., Zhu, S., Yue, J., Zhang, M., Antaris, A.L., Yuan, J., Cui, R., Wan, H., Zhou, Y., et al. (2017). Boosting the down-shifting luminescence of rare-earth nanocrystals for biological imaging beyond 1500 nm. Nat. Commun. *8*, 737.

Zhou, J., Yang, Y., and Zhang, C.Y. (2015). Toward biocompatible semiconductor quantum dots: from biosynthesis and bioconjugation to biomedical application. Chem. Rev. *115*, 11669–11717.

ISCI, Volume *17*

Supplemental Information

Endogenous H_2S-Triggered *In Situ* Synthesis of NIR-II-Emitting Nanoprobe for *In Vivo* Intelligently Lighting Up Colorectal Cancer

Zhiming Deng, Mingyang Jiang, Youbin Li, Hongrong Liu, Songjun Zeng, and Jianhua Hao

Supplemental Figures

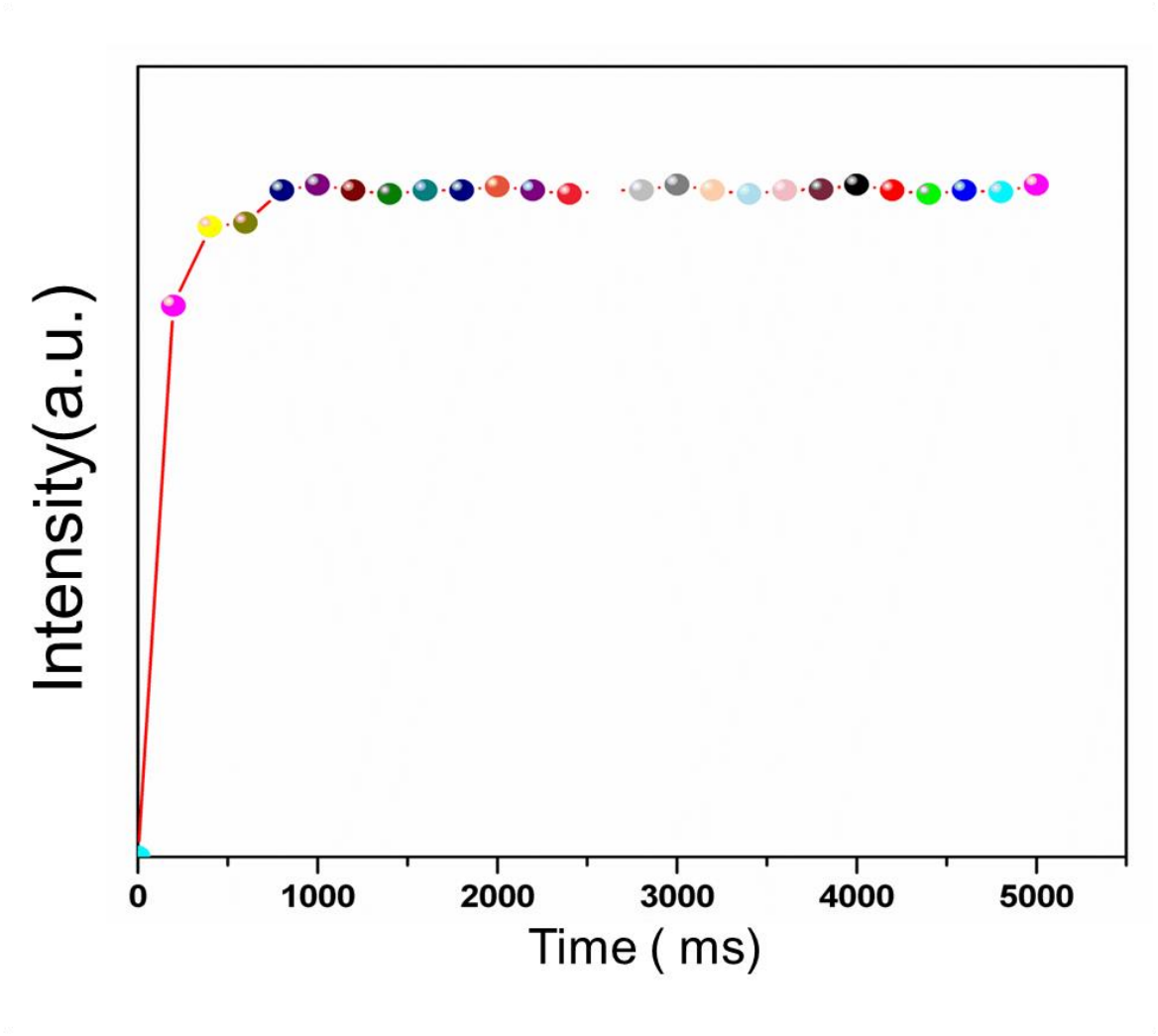

Figure S1. Time-dependent fluorescent changes of Ag-CEW complex with adding Na_2S, related to Figure 1.

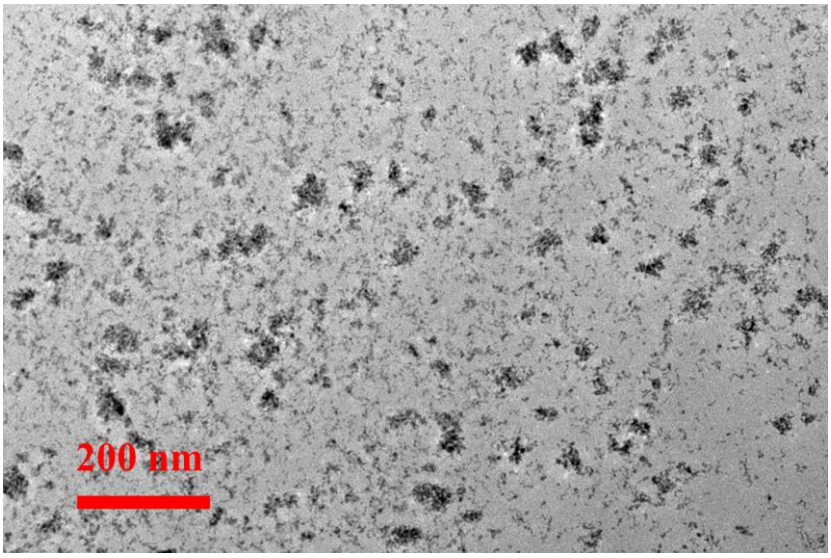

Figure S2. TEM image of CEW modified PbS nanocrystals via the same method as Ag_2S-CEW, related to Figure 1.

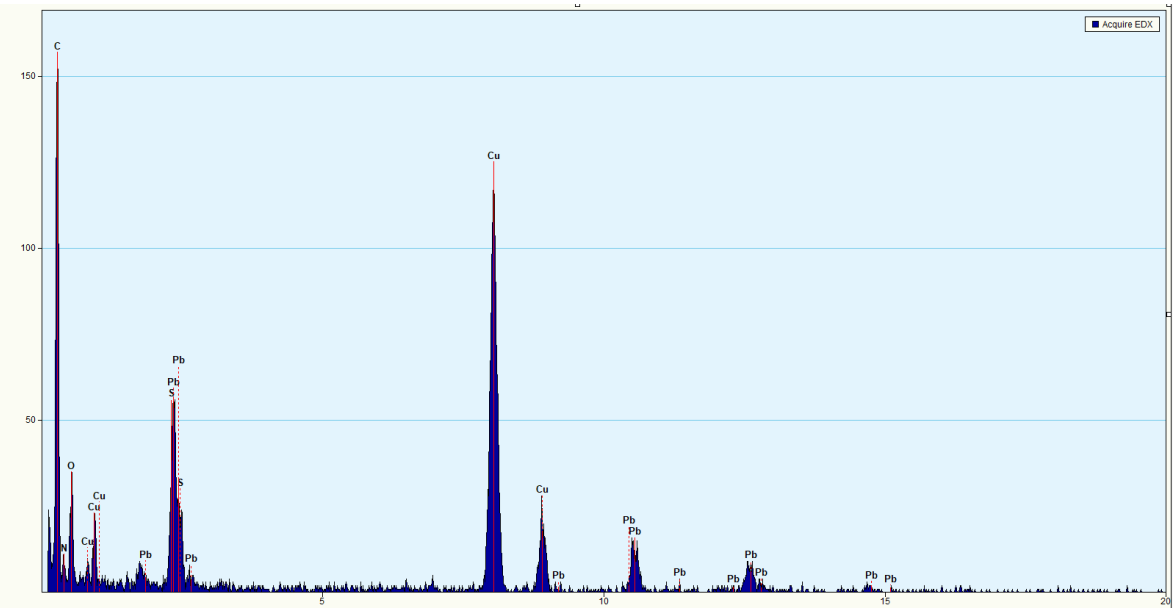

Figure S3. EDS spectrum of CEW modified PbS nanocrystals, related to Figure 1.

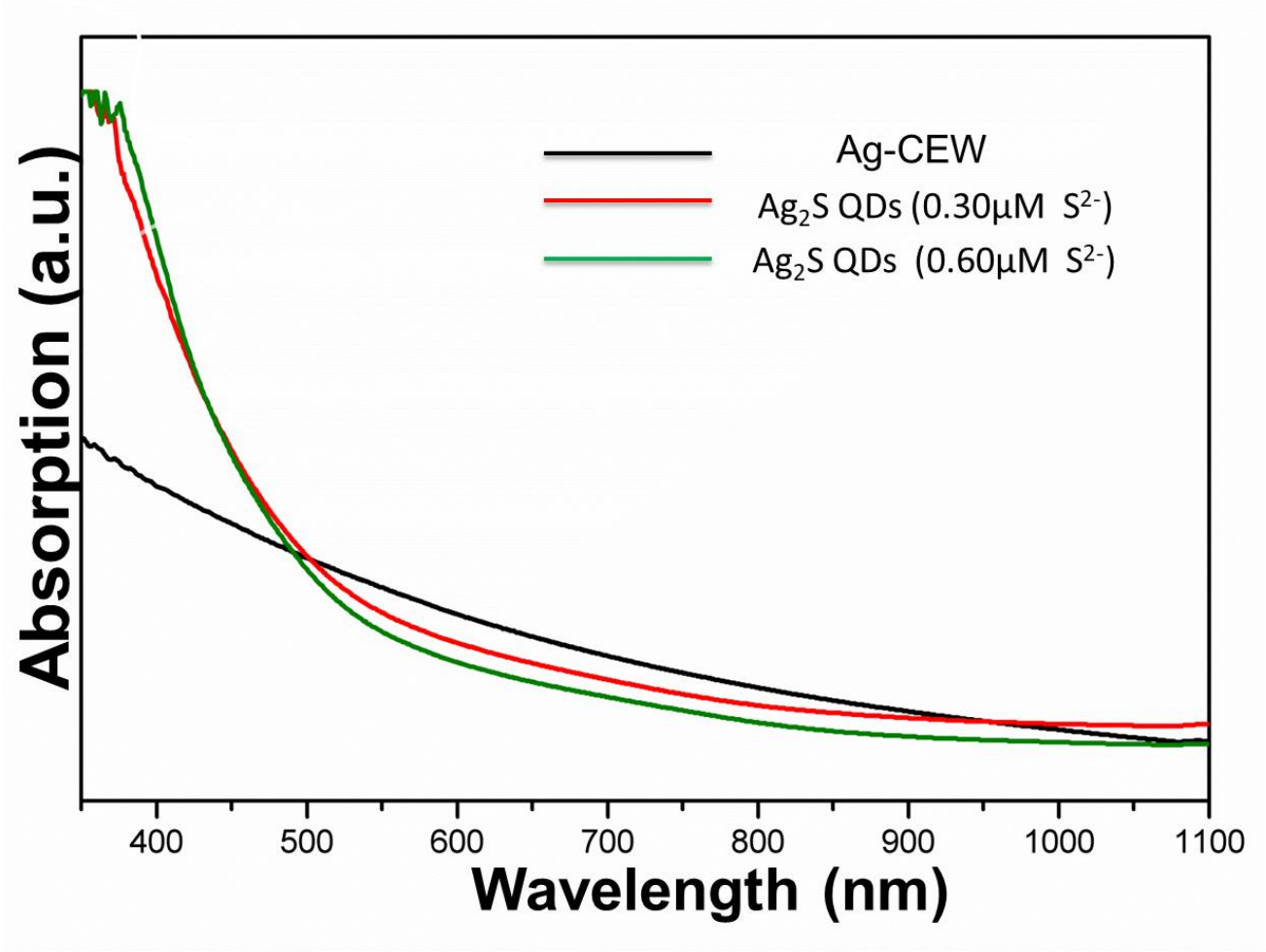

Figure S4. Absorbance spectra of Ag-CEW and Ag_2S-CEW QDs, related to Figure 2.

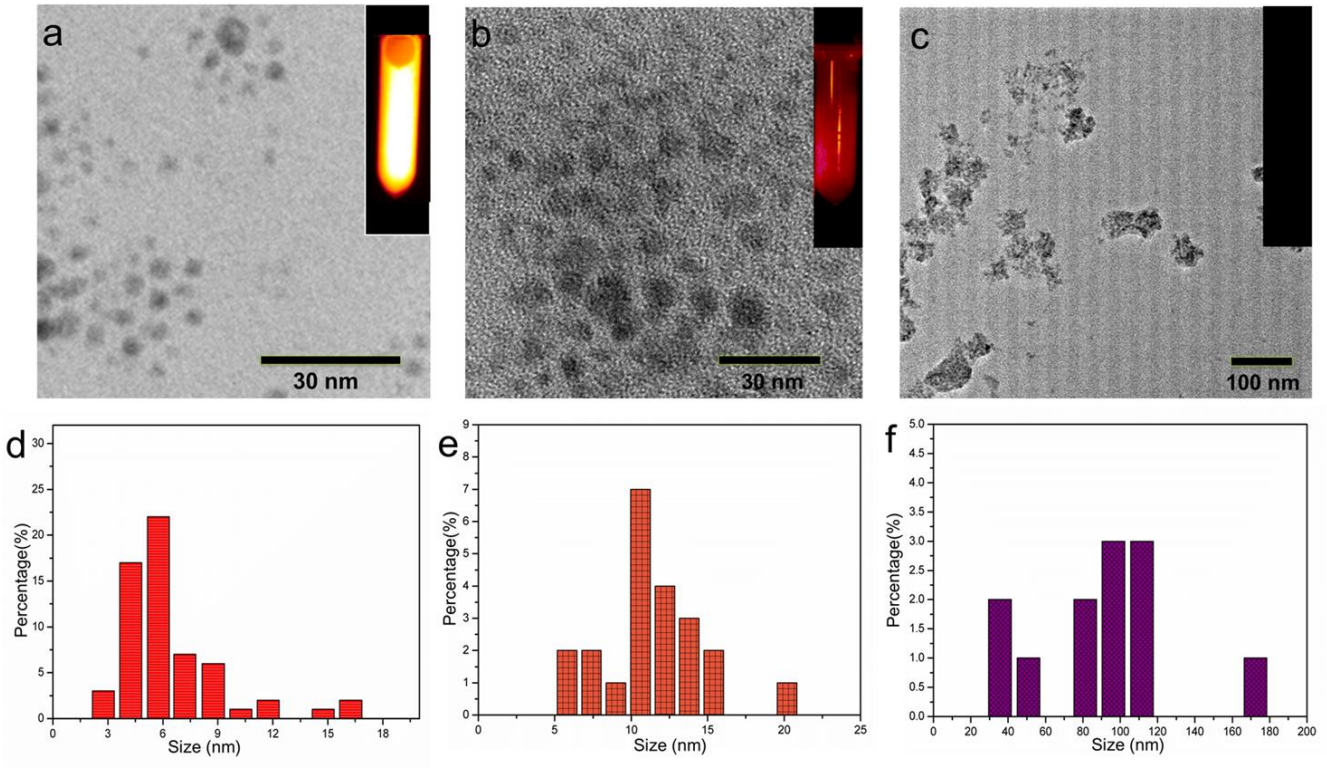

Figure S5. TEM image(a-c) and size distribution histograms (d-f) of Ag_2S nanocrystals with different sizes (inset: *In vitro* phantom NIR-II optical imaging), related to Figure 2.

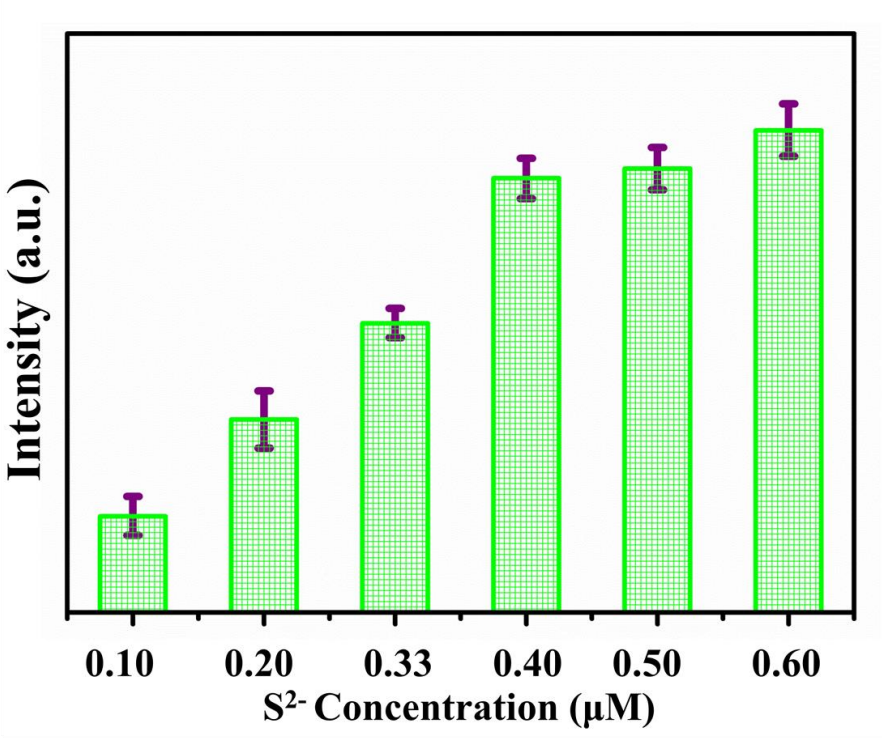

Figure S6. The NIR-II fluorescence intensity of Ag-CEW complex solutions via adding different contents of Na_2S, related to Figure 2.

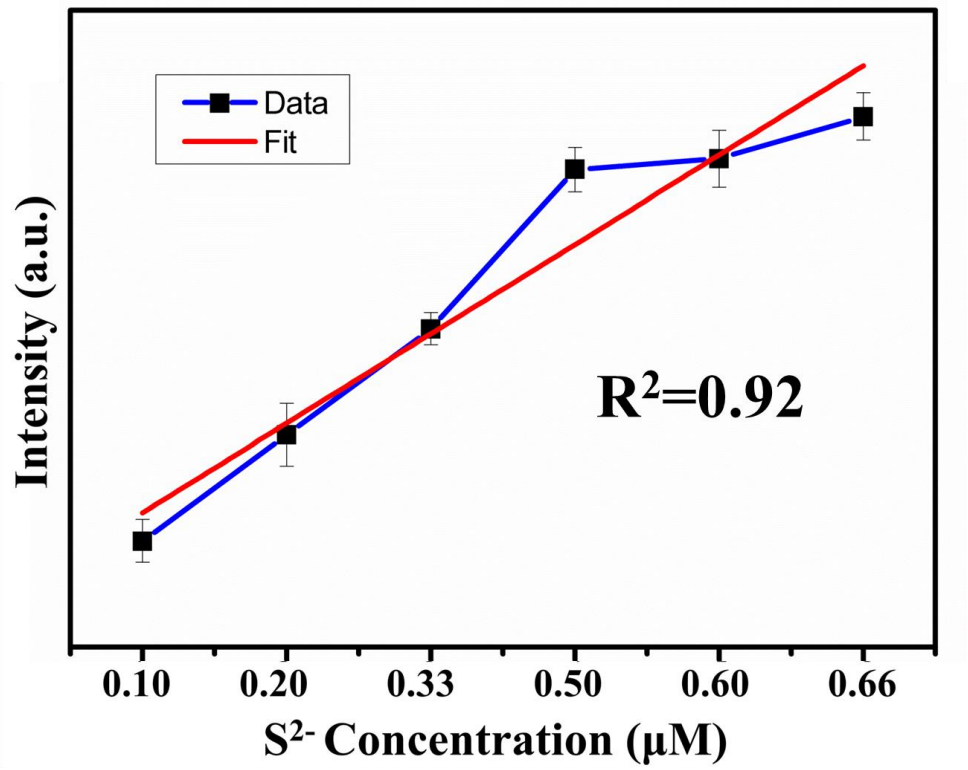

Figure S7. Relative NIR-II fluorescence intensity trends of aqueous Ag-CEW complex in the presence of different contents of S^{2-}, related to Figure 2.

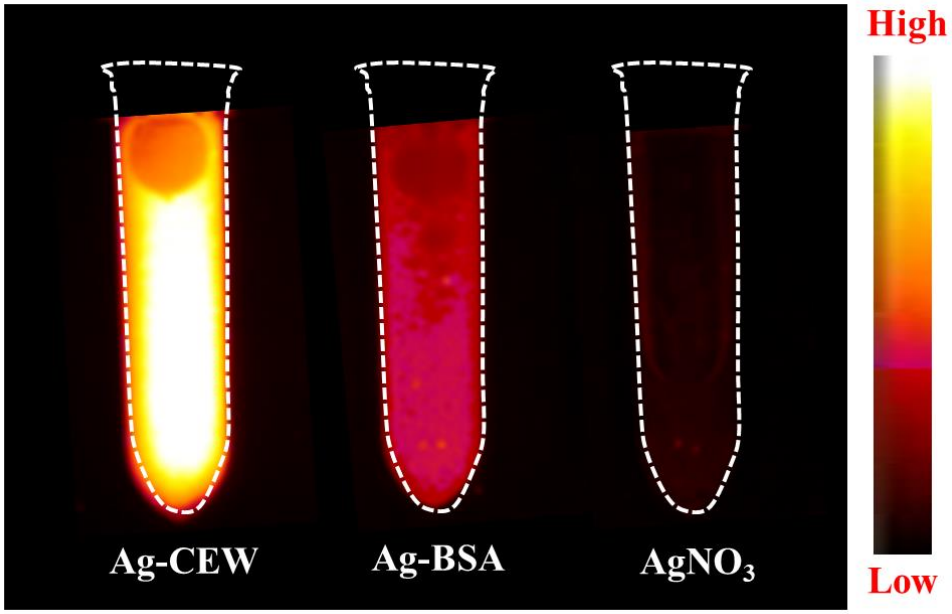

Figure S8. NIR-II optical imaging of Ag-CEW complex, Ag-BSA complex and $AgNO_3$ solution after adding Na_2S, related to Figure 2.

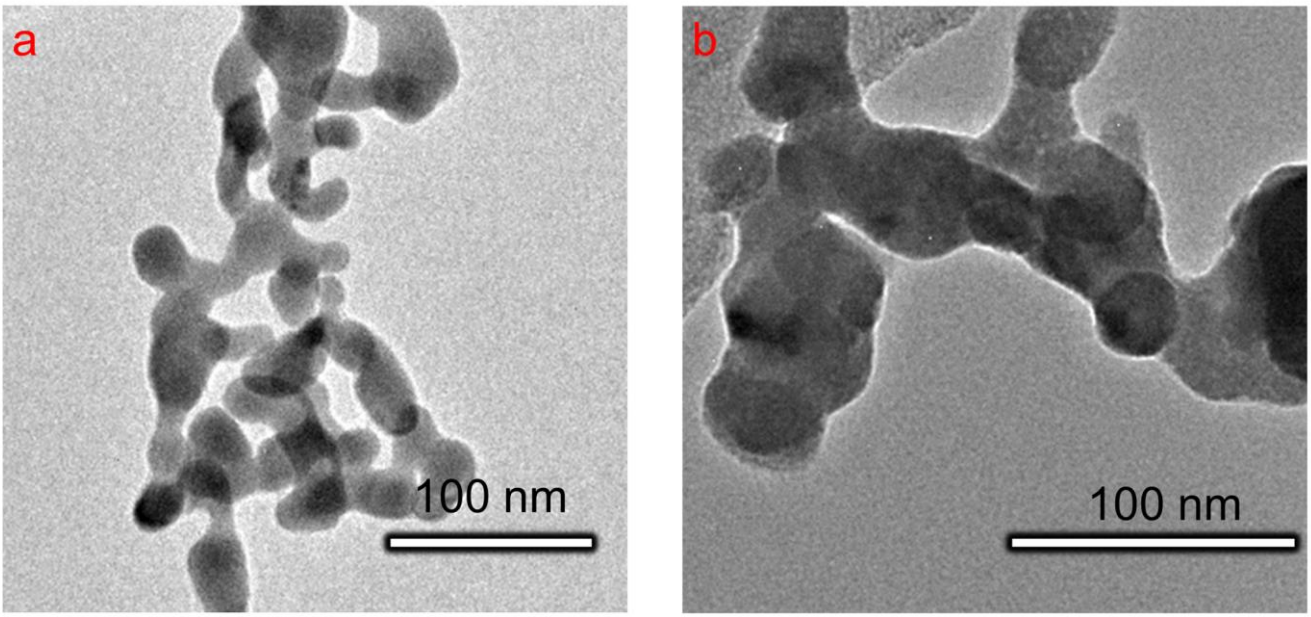

Figure S9. TEM image of Ag_2S nanoparticles achieved from (a) BSA and (b) $AgNO_3$, related to Figure 2.

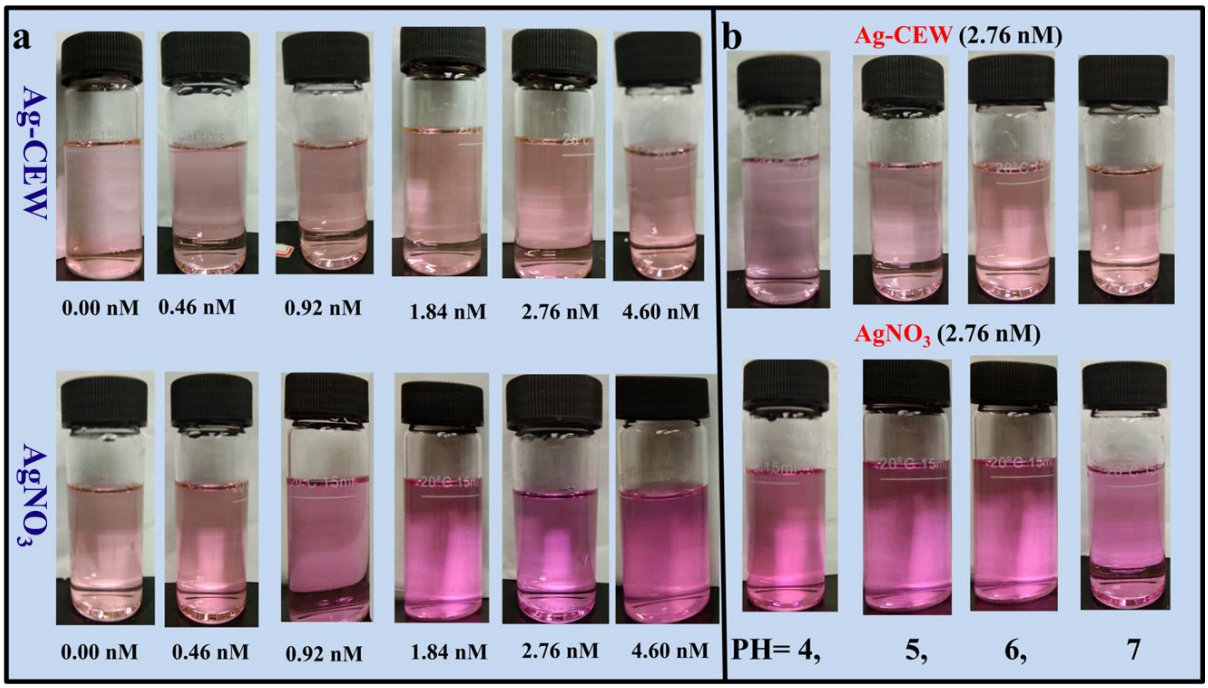

Figure S10. (a) The leakage test of Ag+ in Ag-CEW complex and AgNO3 solutions by using a silver test kit as Ag+ indicator. (b) Silver test kit solution containing Ag-CEW complex (2.76 nM) and Ag+ (2.76 nM) at different pH values, related to Figure 2 and Figure 3.

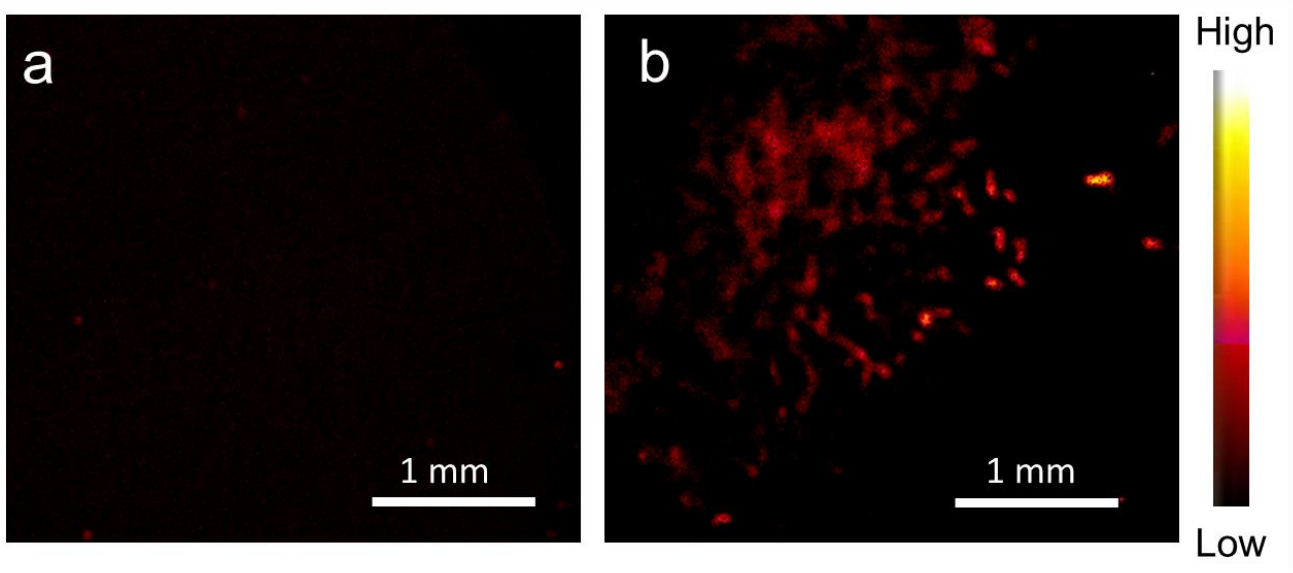

Figure S11. NIR-II fluorescence imaging of HCT-116 cells incubated with PBS (a) and 0.4 μmol/mL Ag-CEW complex (b) for 36 h, related to Figure 3.

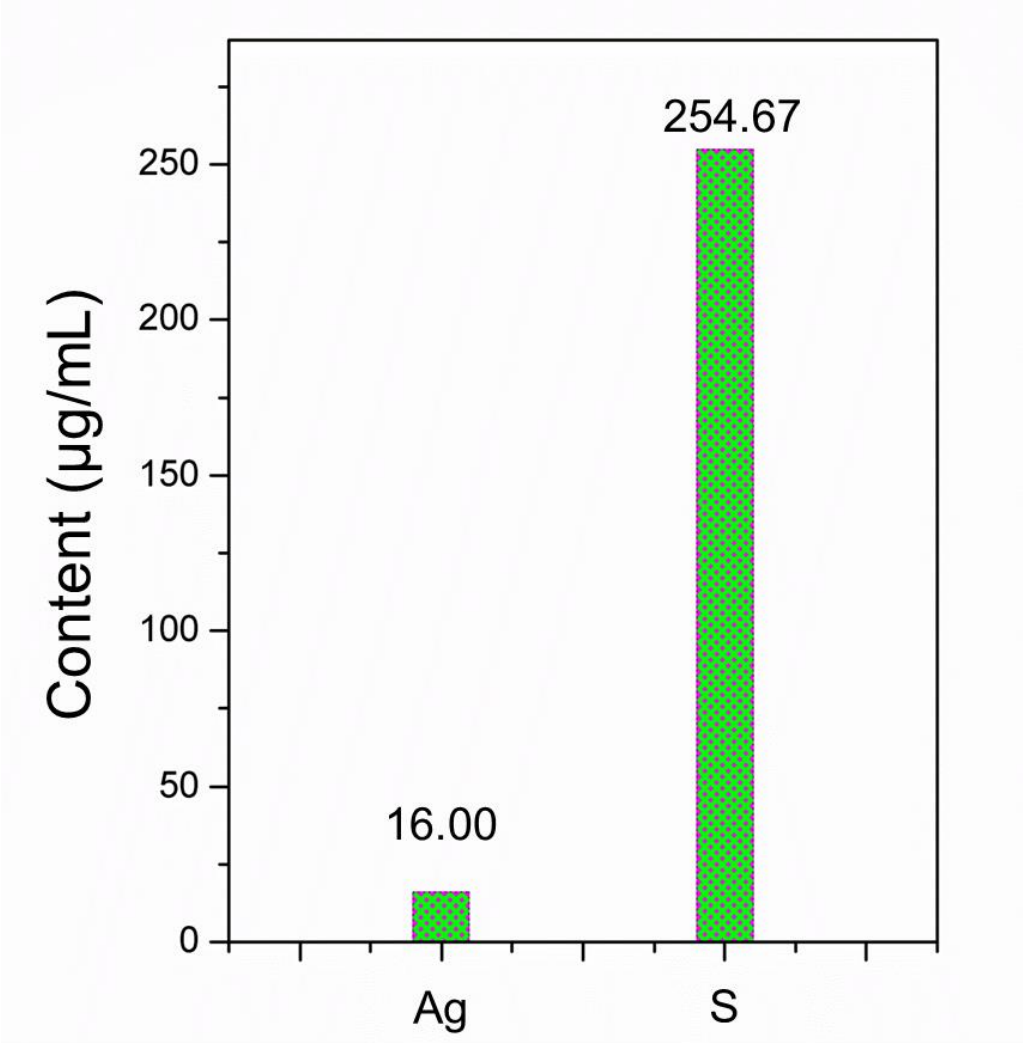

Figure S12. ICP-MS analysis of quantitative contents of Ag and S in tumor tissue, related to Figure 3.

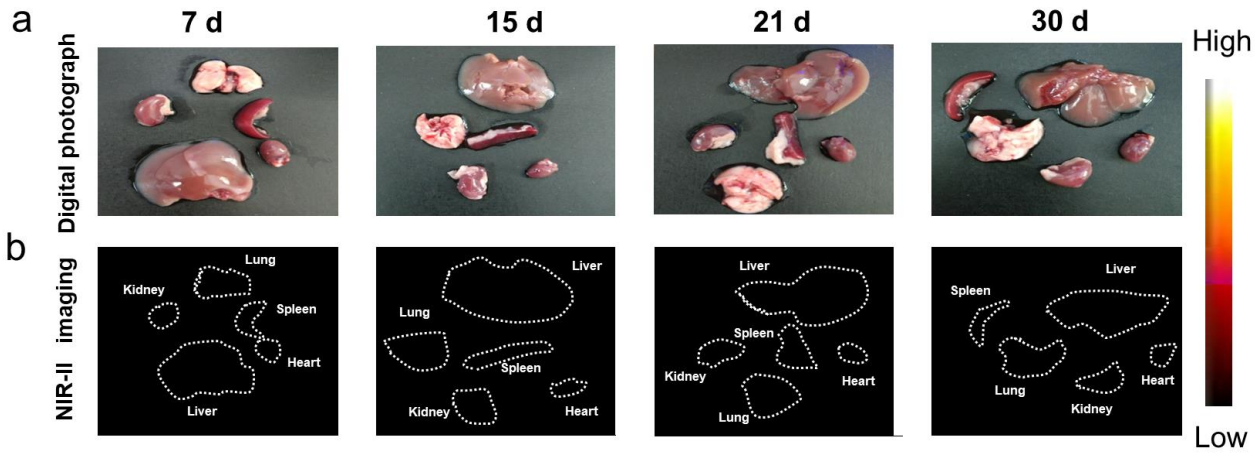

Figure S13. ***Ex vivo*** **NIR-II bioimaging of heart, liver, spleen, lung, and kidneys after intravenous injection of Ag-CEW, related to Figure 3.**

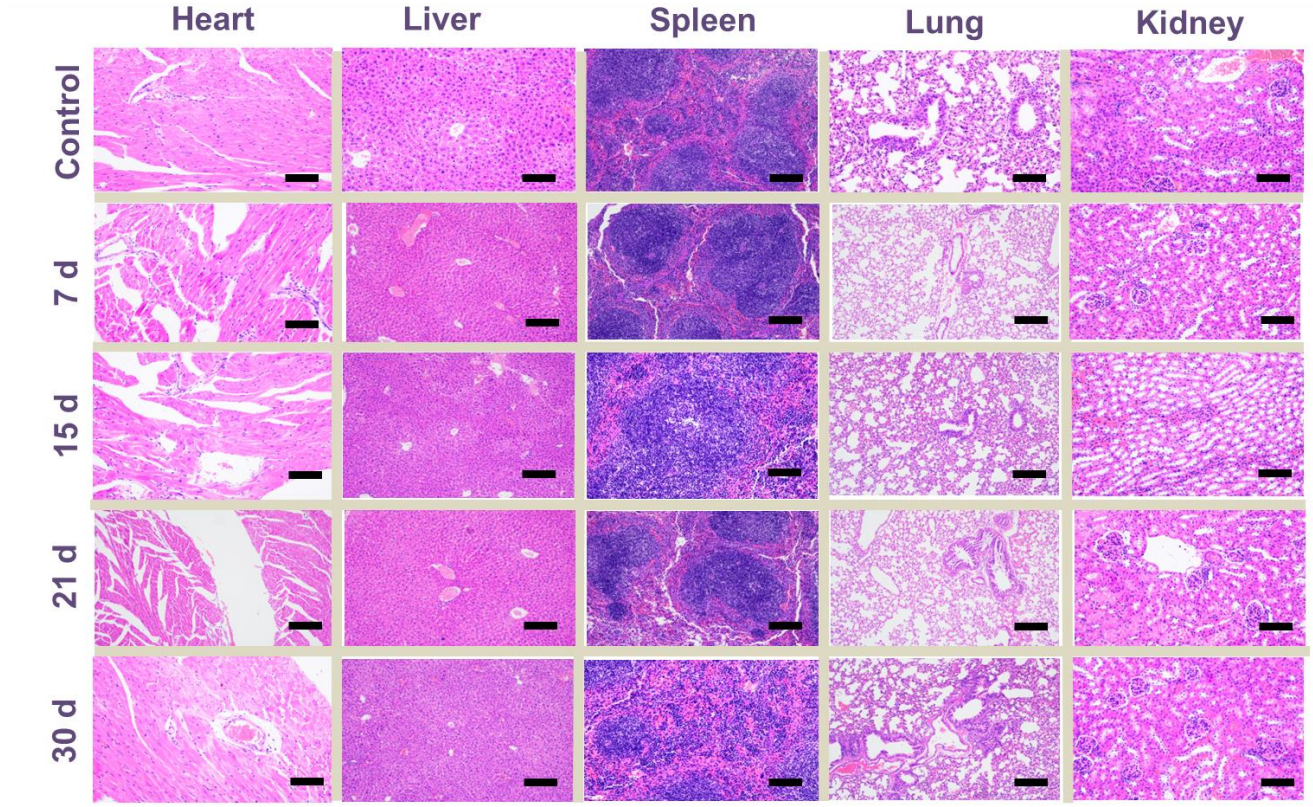

Figure S14 H&E-stained tissue sections including heart, liver, spleen, lung, and kidney retrieved from mice without injection, and after injection of Ag-CEW complex for 7, 15, 21, and 30 days. Scale bars are 100 μm, related to Figure 3.

Transparent Methods

Synthesis of Ag-CEW complex: $AgNO_3$ was analytical pure and used as received from Sinopharm China. Fresh eggs were purchased from a local supermarket. In a typical synthesis process, fresh chicken egg white (CEW) liquid (0.05 mL) was carefully separated from the fresh egg and then dissolved into de-ionized water (40 mL) under magnetically stirring for 20 min. The CEW complex solution was further centrifuged at 5000 rpm for 6 min to obtain a transparent and homogeneous solution. Subsequently, aqueous solution (5 mL) containing $AgNO_3$ (1 mmol) was added to the above CEW complex solution, and the system was magnetically stirred at room temperature for 30 min, obtaining a Ag-CEW complex solution. Ag-CEW complex solution was washed with de-ionized water three times and finally dispersed in de-ionized water and stored at 4 ℃ for further use.

Characterization: X-ray diffraction (XRD) measurements were performed by a Rigaku D/max 2500 X-ray diffractometer with Cu-Kα radiation (λ= 0.15406 nm) at 40 kV and 250 mA. The shape and structure of the as-prepared Ag_2S QDs were characterized by transmission electron microscopy (TEM, FEI Tecnai F20), and high-resolution TEM (HR-TEM) at an acceleration voltage of 200 kV. The element compositions in Ag_2S QDs were analyzed by using X-ray photoelectron spectroscopy (XPS, Thermo Fisher Scientific-Escalab 250Xi). The NIR-II emission was detected by using a NIR spectrometer (NIRQuest512, Ocean Optics) in the 900-1700 nm spectral region under a 808 nm laser excitation. NIR-II optical imaging was acquired by using a home-made NIR-II imaging system(Li et al., 2018; Xue et al., 2018; Li et al., 2019) equipped with a

InGaAs NIR-II detector (Model: NIRvanaTM, Default Operating temperature: -80 ℃, 512×640 pixels, Princeton Instruments) under the excitation of a 808 nm laser.

Quantum yield (QY) measurement of Ag_2S QDs: The QY of Ag_2S QDs in water was evaluated via a similar route to the reported method (**Antaris et al., 2016**) using a standard IR-26 dye (QY = 0.5%) dissolved in 1, 2-dichloroethane (DCE) as a reference. The QY was calculated by the following formula:

$$\Phi_s = \Phi_r(F_s / F_r)*(A_r / A_s)*(n_s^2 / n_r^2)$$

where Φ presents QY, F denotes integrated photoluminescence emission intensity, A denotes absorbance at the maximum excitation wavelength and n is the refractive index of the solvent (n= 1.33 for water, n = 1.44 for DCE, respectively). The subscripts s and r represent the sample and reference solutions, respectively.

***In vitro* cell imaging**: Cellular imaging experiment was conducted. HCT-116 cells were seeded in culture dishes with a density of 5×10^4 cells/mL and incubated at 37 ℃ for 36 h among 5 % CO_2. Then, Ag-CEW complex with concentration of 0.4 μmol/mL was added and incubated for another 36 h, while the control group was injected with equivalent PBS. At last, the cellular images were recorded by the homemade NIR-II imaging system with a field of view of 26 mm × 21 mm (a pixel size of 41 μm) under 808 nm laser excitation.

Tumor models: 8×10^6 colorectal cancer (HCT116) cells and lung cancer (A549) cells were subcutaneously injected into nude mice, after further culturing about four weeks, the tumor-bearing mouse models were obtained for *in vivo* NIR-II optical experiments. All animal procedures in this study were performed in accordance with the Guidelines

for Care and Use of Laboratory Animal Center of Hunan Normal University and approved by the Animal Ethics Committee of Hunan Province.

***In vivo* NIR-II optical imaging based on Ag-CEW complex:** In order to evaluate the *in-situ* reaction of Ag-CEW complex with endogenous H_2S in colon cancer, 200 μL of the Ag-CEW complex aqueous solution (10 μmol mL^{-1}) was subcutaneously injected into the mouse after anesthetization with an intraperitoneal injection of 100 μL of pentobarbital sodium aqueous solution (10 wt%). *In vivo* NIR-II luminescent bioimaging was performed with the NIR-II imaging system under excitation by a 808 nm laser with a power density of 100 mW cm^{-2}.

Histological examination: Kunming mice were divided into two groups. The first group of mice was injected intravenously with Ag-CEW complex for 7, 15, 21, and 30 days as the test group. Untreated mice were used as a control group. The heart, liver, spleen, lung and kidneys were collected from both two groups. These sliced organs were stained with haematoxylin and eosin (H&E) and observed with an optical microscope.

Supplemental References

Antaris, A. L., Chen, H., Cheng, K., Sun, Y., Hong, G. S., Qu, C. R., Qu, S., Deng, Z. X., Hu, X. M., Zhang, B., Zhang, X. D., Yaghi, O. K., Alamparambil, Z. R., Hong, X. C., Cheng, Z., Dai, H. J. (2016). A small-molecule dye for NIR-II imaging. Nature Materials *15*, 235-242.

Li, Y. B., Li, X. L., Xue, Z. L., Jiang, M. Y., Zeng, S. J., Hao, J. H.(2018). Second near-infrared emissive lanthanide complex for fast renal-clearable in vivo optical bioimaging and tiny tumor detection. Biomaterials *169*, 35-44.

Li, Y. B, Zeng, S. J, Hao, J. H. (2019). Non-Invasive Optical Guided Tumor Metastasis/Vessel Imaging by Using Lanthanide Nanoprobe with Enhanced Down-Shifting Emission beyond 1500 nm. ACS nano *13*, 248-259.

Xue, Z. L., Zeng, S. J., Hao, J. H. (2018). Non-invasive through-skull brain vascular imaging and small tumor diagnosis based on NIR-II emissive lanthanide nanoprobes beyond 1500 nm. Biomaterials *171*, 153-163.